Single Camera Tracking of Marker Clusters: Multiparameter Cluster Optimization and Experimental Verification

Sebastian Vogt, Ali Khamene, Frank Sauer
Siemens Corporate Research
Imaging & Visualization Department
755 College Road East
Princeton, NJ 08540, USA
sebastian.vogt@scr.siemens.com

Heinrich Niemann
Lehrstuhl für Mustererkennung
Universität Erlangen-Nürnberg
Martensstr. 3
91058 Erlangen, Germany

Abstract

We have built a system for augmented reality visualization based on a single head mounted tracking camera. The camera includes an infrared illuminator and works in conjunction with a set of retro-reflective markers that are placed around the workspace. This marker frame configuration delivers excellent pose information, which translates to stable, jitter-free augmentation. In this article, we describe using the same single camera system for tracking relatively small marker clusters, which can be used for tool or instrument tracking. Tracking of such a marker cluster is more susceptible to noise compared to tracking of a marker frame, mainly due to its small image coverage. The sensitivity to noise is studied using Monte Carlo simulations and verified in an experimental setup. We achieved jitter-free augmentation with an optimized cluster design.

1. Introduction

Tracking is an essential enabling technology for most of the augmented reality applications. Commercial tracking systems are generally based either on optical or magnetic technologies. Optical trackers achieve higher accuracy, with the requirement of an unobstructed line-of-sight between the tracking camera and the tracked markers. Commercially available optical tracking systems are all based on multiple cameras. They locate the 2D projections of the markers in the camera images and determine their 3D locations by triangulation. Reference [2] provides a survey comparing the basic tracking technologies.

Our prototype AR system uses only a single camera for tracking, which is rigidly attached to the two cameras that capture the stereo view of the scene. Originally, we used this tracking camera — in combination with a set of markers framing a workspace — for determining the pose of the user's head [14, 11, 10, 13, 12]. Mounting the tracking camera on the user's head (also referred to as an *inside out* system [16]) helps with the line-of-sight restriction of optical tracking; the user cannot step into the field of view (FOV) of the tracking camera (though the user still can occlude markers with his or her hands). Placing a forward looking tracking camera on the head is also optimal for the perceived accuracy of the augmentation, as the sensitivity of the tracking camera to registration errors is matched to the user's sensitivity to perceive these errors [6, 3]. Furthermore, this configuration makes good use of the FOV of the tracking camera since tracking is only required when the user actually looks at the workspace. For this reason, the markers framing the workspace can extend over a sizeable part of the image, yielding good tracking accuracy [3].

In this article, we describe how we extend the single-camera tracking to include the tracking of tools with marker clusters attached to them. For practical reasons small marker clusters are more desirable, however since they only extend over a small area in the tracking camera image, the precision of the estimated pose becomes a limiting factor. Therefore, we investigate a suitable design of marker clusters and analyze the relationship between the tracking accuracy and the design parameters. Furthermore, to compare merits of various marker cluster configurations, we consider two forms of error measures, namely the 6D pose estimation error, and the 3D error of a target point within the desired coordinate system of the marker cluster. The benefit of this study is to be able to optimize the marker cluster configuration within the constraints of the application.

The organization of the article is as follows. Section 2 describes the evaluation methods and error measures that we use for the tracking system. Section 3 proposes a suitable marker cluster design and describes the method for analyzing the error for various marker configurations in both

Proceedings of the International Symposium on Mixed and Augmented Reality (ISMAR'02)
0-7695-1781-1/02 $17.00 © 2002 IEEE

simulations and experimental measurements. We then conclude with a summary in Section 4.

2. Single Camera Tracking

In an augmented reality application, computer graphics are rendered onto a real-world video or image sequence. The relative pose (location and orientation) of the video camera to a world coordinate system is necessary to make the computer graphics aligned with respect to some real object in the scene. In other words, we need to know the relationship between two coordinate systems, the one attached to the camera, and the other attached to the workspace [4].

Registration initially establishes this relationship in terms of translation and rotation. Tracking denotes the process of keeping track of these quantities. Single camera tracking is possible when the geometry of the tracked object and the internal camera parameters are known. In this work, we assume the internal camera parameters are pre-estimated utilizing a calibration object, which contains over one hundred markers [14]. We also consider two types of tracked marker sets, namely *frame* and *cluster*, which are explained with more details below.

2.1. Frame Tracking

We fabricate a marker set with retro-reflective disc shaped markers that frames the workspace. The 3D coordinates of the markers are measured beforehand with the commercially available multi-camera tracking system *ARTtrack1* [1]. In order to establish the relationship between the frame coordinate system and the camera coordinate system in real-time, we first need to determine the 2D positions of the projected 3D markers from the tracking camera image. We can then compute the transformation using an external camera calibration algorithm [4]. For this purpose, we utilize Tsai's calibration algorithm [15], that requires at least seven 2D–3D point correspondences. We have achieved very good accuracy using a marker set framing the workspace [14]. The precision is mainly due to the configuration and size of the frame marker set, which covers a large part of the tracking camera image providing good leverage for pose estimation [5]. It is also noteworthy to mention that the frame marker set is designed to extend around the workspace as much as possible, providing good accuracy in the position of the target points all over the workspace.

2.2. Cluster Tracking

We refer to the cluster marker set as a marker set that, unlike the frame maker set, does not extend over the workspace. It is usually used for tracking an auxiliary tool or instrument. The same principle as discussed in Section 2.1 can be applied for tracking this kind of marker set. However, there are some challenges for marker based tool tracking. For practical reasons, the marker cluster that is attached to the hand-held tool should be small. However, for a single camera tracking system, miniaturizing the marker set could considerably decrease tracking accuracy [5]. This limitation is less crucial in a multi-camera tracking system. In this article, we will analyze coplanar and non-coplanar marker clusters. Tracking of coplanar clusters of markers has been studied for a variety of applications, e.g. in [7, 9, 17].

2.3. Tracking Error

In photogrammetry the *exterior orientation* problem describes the problem of determining the pose of a rigid body, given an image from a single camera [6]. The outcome of a pose estimation algorithm (i.e., external camera calibration) is a 6D quantity encoding the translation and rotation. From the error of the 6D pose estimation we can deduce the 3D position error of a target point in the frame or cluster coordinate system in two forms. The first is a *biased (systematic) error*, which is the deviation of the mean of the 3D position from the true value. The second is a *jitter*, which is the variation of the 3D position in time around the mean position.

We assume that the biased pose error is related to the internal calibration accuracy, the precision of the 3D coordinates of the marker set, any bias that exists in the estimates of 2D location of the projected markers in the tracking camera image, and any biased error in the 3D–2D matching (pose estimation) algorithm. Also, because of the non-linear nature of the projection, any unbiased noise in the pose values reflects a biased error in the 3D position.

Studying the biased error in the 3D position of a target point is a challenging subject. This is mainly because the dimension of the parameter space for the problem is quite high [8]. In this article, our primary goal is to achieve a jitter-free and stable overlay in an AR setup. Therefore, we only consider the jitter error, which is dominantly caused by the error of the estimation of the 2D marker locations in the tracking camera image. By characterizing this error, we are able to estimate the resultant error of the pose and consequently predict the amount of jitter in the 3D position of any target point. We assume that the biased error is negligible mainly under the assumption that the parameters affecting the biased error are pre-calibrated off-line and can be acquired with high degrees of accuracy.

To compare merits of various marker cluster configurations, we consider two forms of error measures:

- the 6D pose estimation error (jitter of calculated rotation and translation), and

- the 3D error of a target point within the desired workspace of the marker cluster.

The first form is the most comprehensive for error evaluation, whereas the second item is only focused on the errors in the target point(s) and thus more intuitively comprehensible. For instance, an error distribution in the position of a target point can readily be presented by a 95% confidence ellipsoid. It is also noteworthy to mention that the overlay (augmentation) jitter of the projected target point onto an arbitrary plane can be extracted using the 3D error distribution of that point.

In the next section, we first identify the variation of the extracted 2D locations of the centers of the projected markers in the camera image and then analyze the error measures discussed above for different marker cluster configurations using Monte Carlo simulations and real experiments.

3. Design Study

Single camera tracking of hand-held tools becomes possible by attaching marker clusters as denoted in Section 2.2. Utilizing Tsai's calibration technique for estimating the 6D pose of an object requires to establish at least seven 3D–2D point correspondences. Therefore, it is necessary to design a cluster of at least 7 markers that can be rigidly affixed to the tool in a way that all markers are visible in the tracking camera, i.e., they should not overlap or be hidden by the tool or cluster construction itself. Furthermore, the identification of the projected markers in the image of the tracking camera should be possible in order to establish the right correspondences to the real markers in the cluster.

Given the exact 3D locations of the markers in their own coordinate system and the 2D locations of the marker projections in the tracking camera image as input for Tsai's calibration technique leads to the rigid body transformation between the marker cluster coordinate system and the camera coordinate system, i.e., the 6D pose of the marker cluster. Thus, three groups of input parameters influence the result of the pose estimation:

- the internal parameters of the tracking camera,
- the 3D coordinates of the markers in the cluster coordinate system, and
- the 2D coordinates of the projections of the markers in the tracking camera image.

On one hand, it is necessary to precisely determine these input parameters to achieve good accuracy for the pose estimation. Assuming fixed internal camera parameters and rigidly mounted markers, only the last item, i.e., the extraction of the 2D coordinates from the camera image, becomes a crucial factor during the real-time tracking of the marker cluster. Pixel jitter in the camera image therefore directly affects the stability of the estimated 6D pose. To what extent this 2D jitter translates into a jitter of the 6D pose of the marker cluster (and the attached tool) depends, on the other hand, also on the design of this cluster.

Analyzing the influence of the structure of the marker cluster on the stability of its estimated 6D pose is the major interest in this presentation of our work. In the following sections, we will illustrate how a suitable marker cluster can be constructed and how we evaluated a family of clusters in computer simulations and experimental measurements in terms of the error measures discussed in Section 2.3.

3.1. Marker Cluster Design

The distribution of markers in a cluster is constrained by the fact that all of them must be visible in the camera image over a wide range of cluster poses without possible occlusions. Furthermore the size of the cluster should be small enough to be easily attached to the hand-held tool.

Marker based tracking usually utilizes either spherical or disc shaped markers. For our investigations we choose disc shaped markers since they are easy to produce by punching them out of a sheet of retro-reflective material. We consider marker clusters with markers located on the perimeter of a circle, in various heights relative to the plane of the circle. Additionally, one marker is placed in the center of the circle. On one hand, a symmetric marker distribution presumably leads to a symmetric error distribution in the x- and y-direction of the marker cluster coordinate system. On the other hand, this cluster design allows a simple identification of the markers in the camera image, since a view from the top at this marker cluster reveals its circular structure. For labeling we have one marker with a greater diameter, whereas all the other markers have the same size. A schematic representation of this marker configuration is illustrated in Figure 1.

Figure 1 shows also a captured image of the tracking camera, which is only sensitive in the near-infrared spectrum. The retro-reflective markers which are illuminated by near-infrared light give a very good contrast in the camera image and therefore allow an efficient and accurate localization. The eight smaller markers in the lower part of the image belong to the tracked marker cluster, whereas the nine larger markers are the ones that frame the workspace as described in Section 2.1.

We choose three parameters to characterize the introduced family of marker clusters:

- the number of markers,
- the radius of the circle, and
- the maximum height of a marker compared to the plane of the circle.

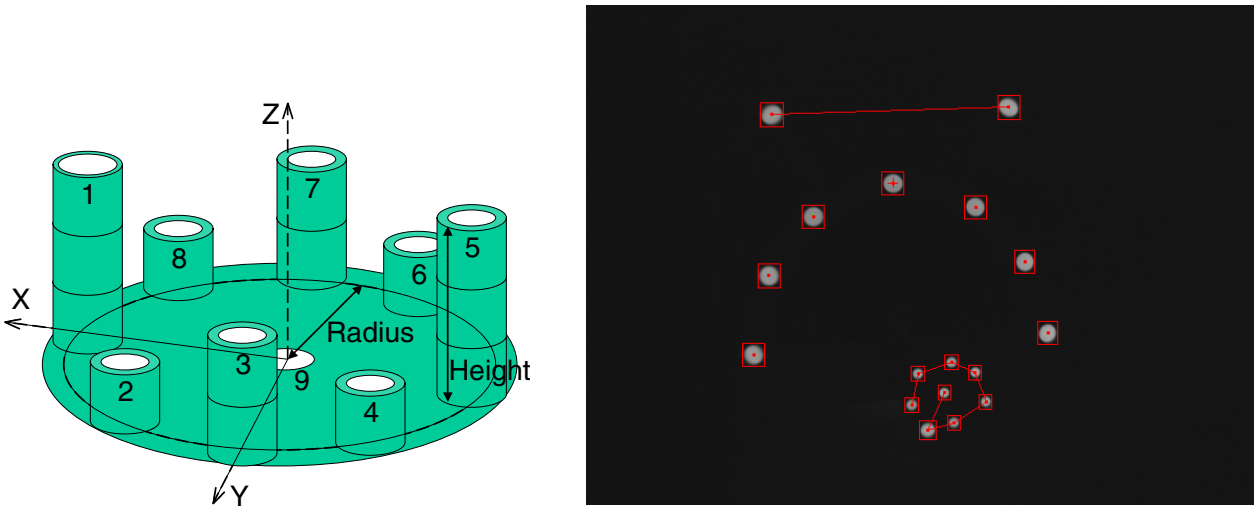

Figure 1. *(left)* **Schematic representation of the design of the introduced family of marker clusters. The markers (in white) are rigidly mounted on little posts that are arranged in a circular shape. The circle base lies in the x-y plane of the marker cluster coordinate system.** *(right)* **Image of the tracking camera while tracking the markers, which frame the workspace, and the marker cluster, which is attached to a hand-held tool.**

The last item represents the degree of non-coplanarity and indicates how the markers are distributed in height.

In the next sections we will investigate the influence of the marker cluster design on the tracking error as denoted in Section 2.3 with simulated data and then verify the results in real experiments.

3.2. Design Evaluation Steps

At first we measure and characterize the jitter of the 2D locations of the projected markers in the real image of the tracking camera for different marker sizes and positions.

Assuming an unbiased Gaussian distributed error around the true 2D marker locations, we then use this information to investigate the outcome of the pose estimation based on a simulated 2D projection of a variety of synthesized 3D marker clusters. This is done by modelling 3D marker clusters inside the computer and projecting the 3D marker centers under certain poses into the image plane by using the camera model of our real tracking camera. After adding synthetic noise, which is defined through the prior real observations, to the 2D data of the projected marker centers, we estimate the 6D pose of the marker cluster with Tsai's calibration method as used in our real tracking system. In our work, we represent the 6D pose by the 3 Cardan angles $(\theta_x, \theta_y, \theta_z)$ for the rotation and a 3D vector $(\boldsymbol{t} = [t_x, t_y, t_z]^T)$ for the translation part of the rigid body transformation:

$$\boldsymbol{p}_c = \boldsymbol{R}\boldsymbol{p}_m + \boldsymbol{t} \quad \text{with} \quad \boldsymbol{R} = \boldsymbol{R}_z\boldsymbol{R}_y\boldsymbol{R}_x \quad . \qquad (1)$$

Thereby, $\boldsymbol{p}_m \in \mathbb{R}^3$ and $\boldsymbol{p}_c \in \mathbb{R}^3$ stand for the 3D coordinates of a point in the marker cluster coordinate system and the camera coordinate system, respectively. The rotation $\boldsymbol{R} \in \mathbb{R}^{3\times3}$ is described by a sequential rotation around the three coordinate axes according to the specified Cardan angles. The z-axis of the camera coordinate system is aligned with the optical axis of the camera and points into the scene. Figure 1 illustrates the marker cluster coordinate system.

We quantify and analyze the error measures introduced in Section 2.3 for a variation of the marker cluster parameters and a variation of different poses. Additionally, we also build two marker clusters — one coplanar and one non-coplanar — and measure the deviations in the pose estimation for each of them in an experimental setup.

3.3. 2D Single Marker Jitter

In this first stage, we use single markers of different sizes and analyze the jitter of the extracted 2D locations in the image of our tracking camera. The method for determining the center of a projected marker in the camera image with sub-pixel accuracy is based on calculating the center of gravity of the gray values inside a rectangular bounding box around the extracted 2D marker after background subtraction. Because the only visible objects in the camera image are actually the markers, we use a simple way to eliminate the background by finding the mean of the gray values on the bounding box and subtracting it from all pixels inside the bounding box. This method for extracting the

Table 1. Attributes of the investigated marker clusters.

Attribute	*Series 1*	*Series 2*	*Series 3*	*Series 4*	*Series 5*
Cluster height	0...45 mm	30 mm	30 mm	0 mm	30 mm
Cluster radius	45 mm	15...60 mm	45 mm	45 mm	45 mm
Number of markers	8	8	7...16	8	8
Cluster pose	fixed	fixed	fixed	variable	variable

center of a projected marker utilizes all the available image information in an efficient way.

We choose a setup where several markers in a stationary pose are projected into the image of the tracking camera. The range of the bounding box size is 80 to 1200 square pixels for the projected markers. After taking several thousand measurements for a variety of marker sizes, we conclude that the noise in the extracted 2D coordinates of the centers of the projected markers decreases insignificantly with an increased size of the projected marker in the image. Furthermore, the correlation factor for the noise in the horizontal and vertical coordinate is about 0.4 to 0.6. The noise for different markers of a marker cluster is also correlated with a correlation factor of 0.4 to 0.6. The standard deviation of the noise of the horizontal and vertical coordinate consistently varies from 0.013 to 0.010 pixel for a bounding box size of 80 to 1200 square pixels.

We assume that the measured 2D jitter is caused by the tracking hardware, i.e., mainly the video digitizer board and the tracking camera itself. Consequently, a jitter in the gray values causes a jitter of the calculated 2D marker centers in the camera image. The tests show that the image size of the projected marker seems not to be an important factor so long as the marker spans over several pixel rows and columns in the camera image. One reason might be the fact that the gray values inside the projected marker are mainly saturated (i.e., they have a value of 255) whereas the peripheral gray values are distributed between 0 and 255 and thus susceptible to pixel jitter.

3.4. Simulated Variation of Cluster Parameters

To study the sensitivies to noise using Monte Carlo simulations, we synthesize 3D marker clusters with different radii, heights, and numbers of markers. At each series of experiments one of the three parameters of the marker cluster is changed while the other two are kept constant. Table 1 shows the chosen values (Series 1 to 3). The internal parameters of our real tracking camera are known through a previous calibration procedure and used to model the camera in our simulations. The external pose is the same for each investigated marker cluster, with $\theta_x = 10^\circ$, $\theta_y = 5^\circ$, $\theta_z = 0^\circ$, $t_x = 0\,\text{mm}$, $t_y = 5\,\text{mm}$, $t_z = 500\,\text{mm}$. It is a typical configuration when a marker cluster is attached to a hand-held tool.

This first set of experiments is done to observe the effect of each parameter of a marker cluster on the overall accuracy. It includes the mentioned three scenarios where in each of them only one parameter changes. After projecting the synthesized 3D marker cluster into the image plane of the modeled tracking camera, we add various (i.e., 10000) samples of noise to the 2D locations of the simulated projections of the marker centers based on the experimentally determined noise characteristics as explained in Section 3.3.

The measured variation of the estimated pose is depicted in Figure 2. The top row plots in Figure 2 show the translational variation in millimeter and the bottom row plots the rotational (i.e., Cardan angles) variations in degree. The three columns in Figure 2 represent the results of the three test series with marker cluster parameters according to the columns of Table 1 (Series 1 to 3).

Figure 3 illustrates how the variation in pose in Figure 2 translates into a variation of the 3D coordinate of a target point in the coordinate system of the tracking camera. The target point is chosen to be about 173.2 mm away from the center of the marker cluster coordinate system at [-100 mm, -100 mm, -100 mm]. Figure 3 contains three columns for each of the parameter variations. The top row illustrates the projection of a 95% confidence ellipsoid into the x-y plane and the bottom row shows the projection of the same ellipsoid into the y-z plane of the tracking camera coordinate system assuming a right handed system with the z-axis as the optical axis pointing into the scene. Different ellipses with various shades of gray indicate the variation of the parameter of the marker cluster, whereby brighter ellipses correspond to a higher parameter value.

Referring to Figure 2, it is obvious that the height of the marker cluster, i.e., the distribution of the markers in all three dimensions, is crucial for the accuracy of the estimated tilt of the x-y plane of the camera coordinate system against the x-y plane of the marker cluster coordinate system. The standard deviations of the errors in the rotation angles θ_x and θ_y significantly decrease when the markers of the cluster are better distributed in 3D space instead of being coplanar. Figure 2 further reveals the fact that the jitter of the center of the marker cluster (represented by the translation vector $\boldsymbol{t}$) is mainly along the line-of-sight of the tracking camera. This error can be reduced by using larger marker clusters.

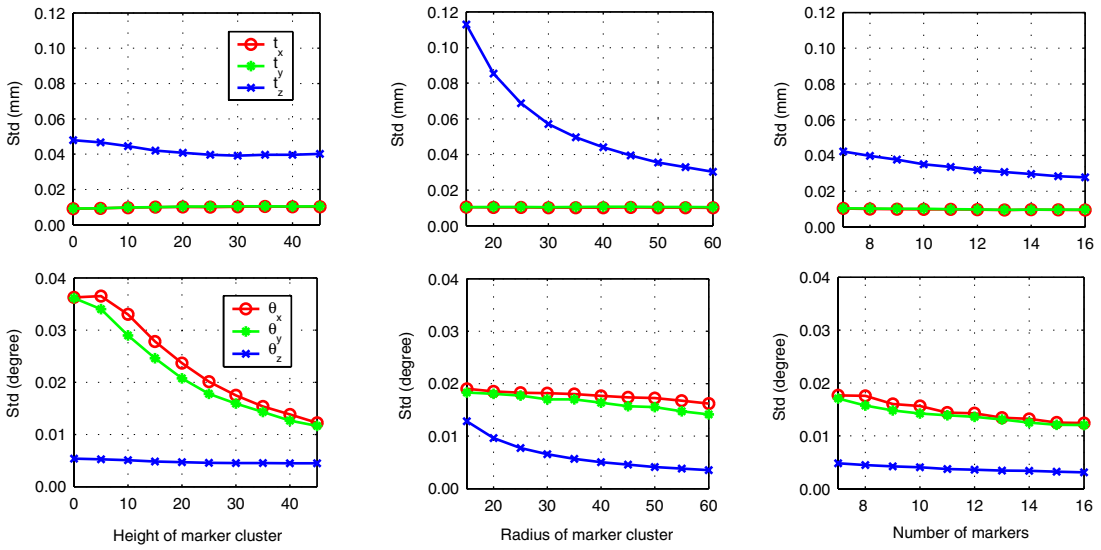

Figure 2. Simulation error plots for the estimated pose, i.e., *(top)* translation and *(bottom)* rotation, for changes in the characteristics of the synthesized marker cluster, i.e., *(left)* height, *(middle)* radius, and *(right)* number of markers.

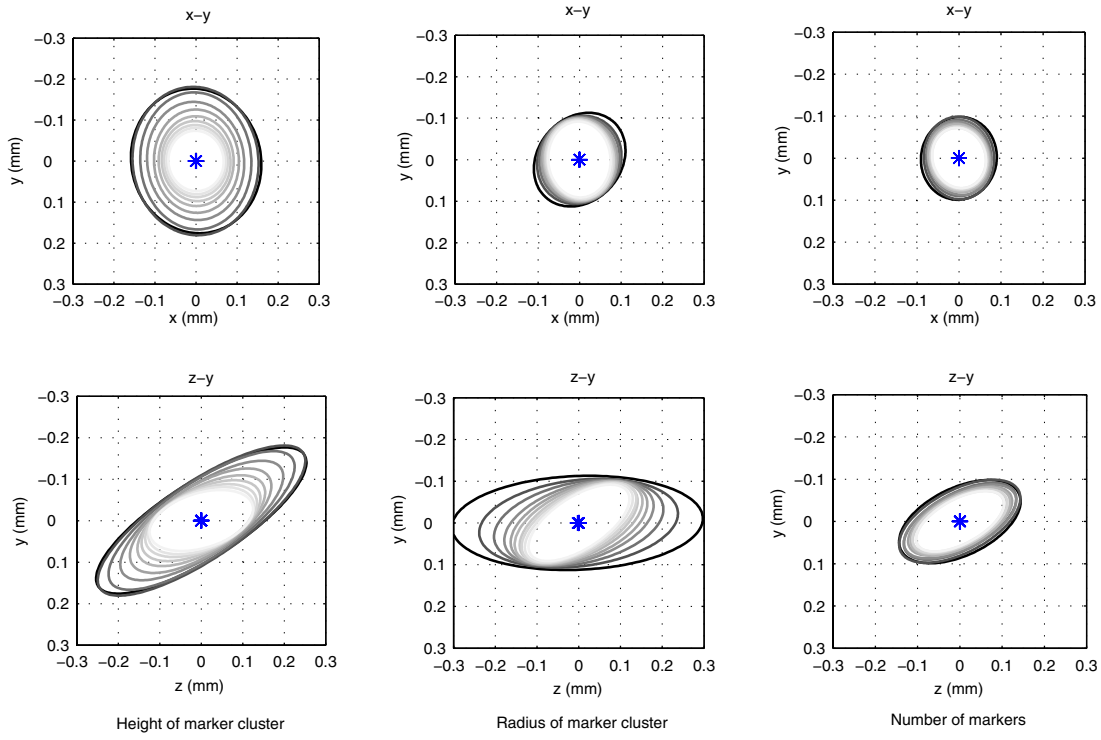

Figure 3. Projection of the 3D 95% confidence ellipsoid for a target point ([-100 mm, -100 mm, -100 mm] in the marker cluster coordinate system) into the *(top)* x-y plane and *(bottom)* y-z plane, for changes in the characteristics of the synthesized marker cluster, i.e., *(left)* height, *(middle)* radius, and *(right)* number of markers. The brightness of the ellipse corresponds to the changing variable along the horizontal coordinate axis in Figure 2.

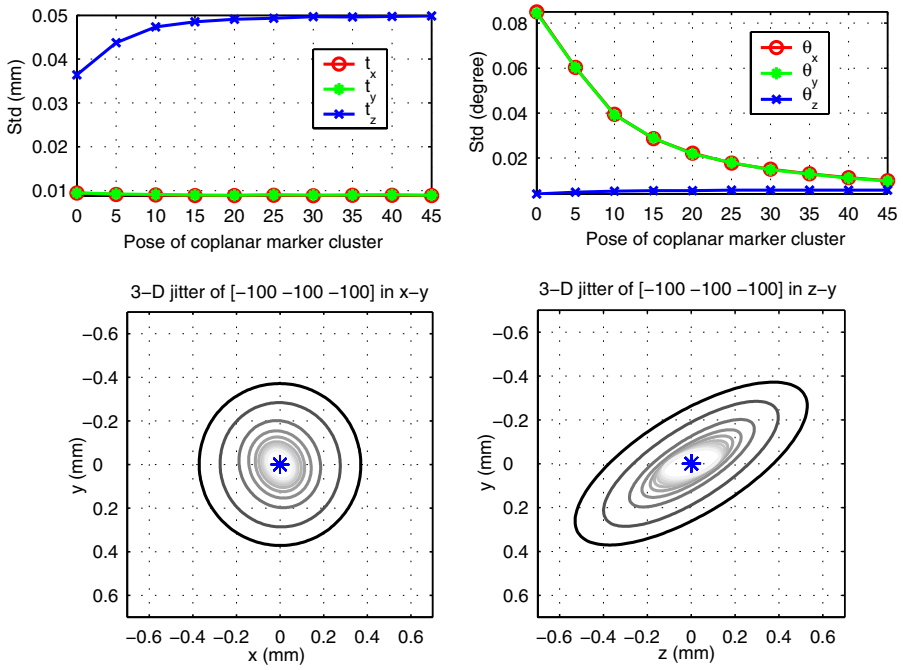

Figure 4. Simulation error plots for the estimated pose of a coplanar marker cluster for various poses, i.e., *(top left)* translation error and *(top right)* rotation error. The horizontal coordinate axes show the tilt of the circle plane of the marker cluster against the tracking camera plane in degree. The bottom figures show the projection of the 3D 95% confidence ellipsoid for a target point ([-100 mm, -100 mm, -100 mm] in the marker cluster coordinate system) into the *(bottom left)* x-y plane and *(bottom right)* y-z plane.

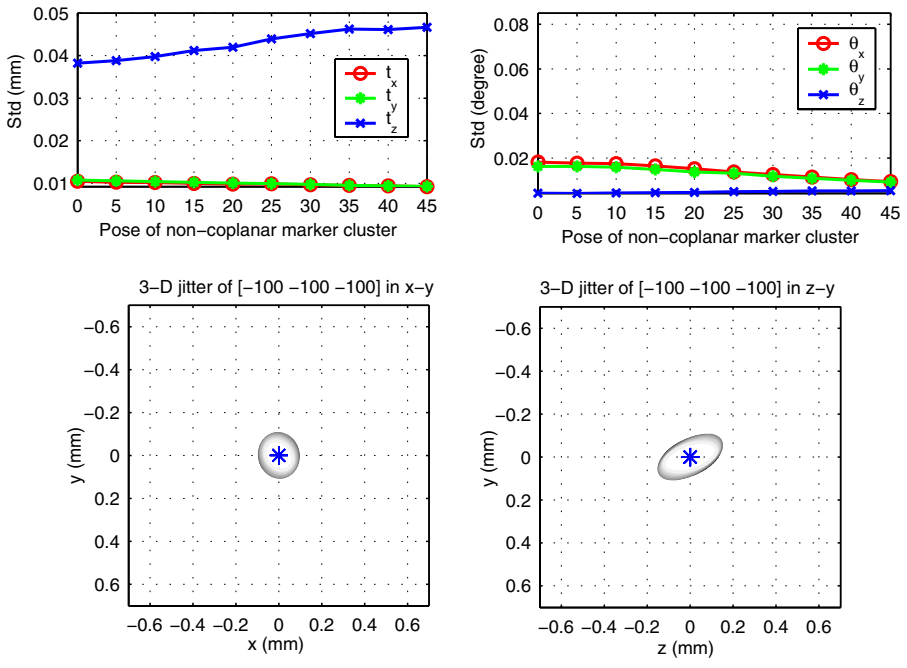

Figure 5. Simulation error plots for non-coplanar marker cluster. Description analogous to Figure 4.

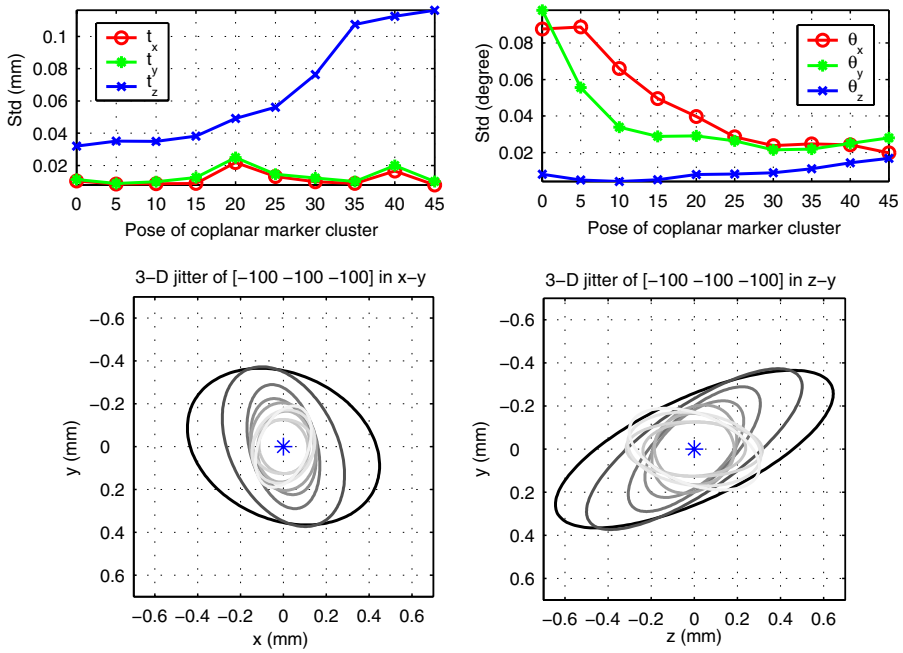

Figure 6. Error plots for real coplanar marker cluster. Description analogous to Figure 4.

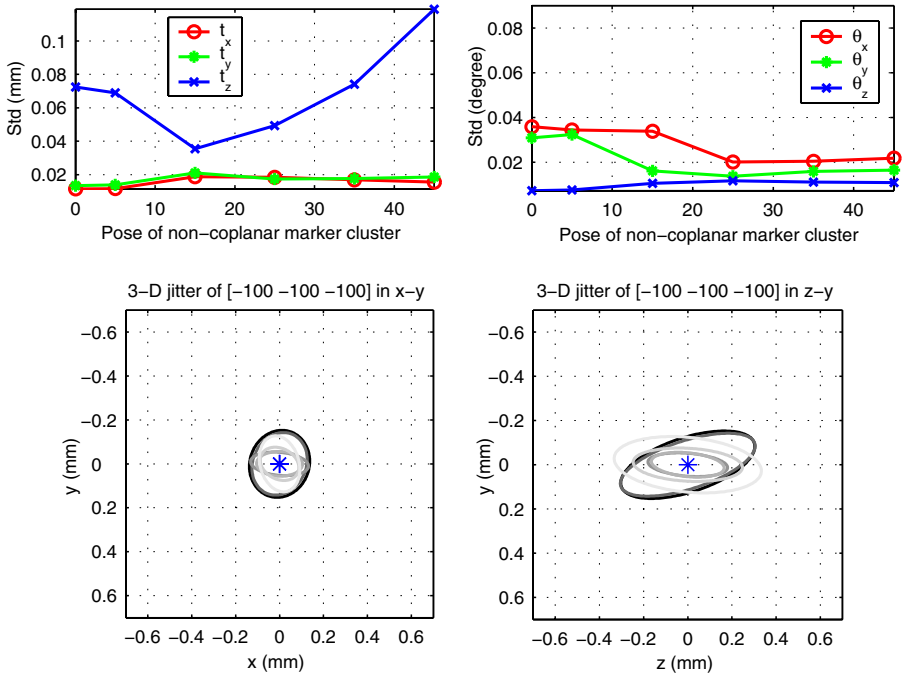

Figure 7. Error plots for real non-coplanar marker cluster. Description analogous to Figure 4.

3.5. Simulated Variation of the Cluster Pose

The second set of simulations uses two specific marker clusters, one coplanar and one non-coplanar, to investigate how the errors depend on the cluster pose. Series 4 and 5 in Table 1 refer to these marker cluster configurations, respectively. We simulate a variation in the pitch angles (i.e., θ_x) from 0˚to 45˚, i.e., starting in a parallel configuration of the camera plane and the plane of the marker cluster circle we stepwise tilt the marker cluster — keeping the center at the same location — until the planes reach a 45˚angle to each other. Then, we repeat the same procedure as explained in Section 3.4 to determine the error plots for the pose and consequently the 3D 95% confidence ellipsoid for the target point ([-100 mm, -100 mm, -100 mm] in the marker cluster coordinate system). These sets of plots are depicted in Figure 4 and Figure 5 for the synthesized coplanar and non-coplanar marker cluster, respectively.

The graphs show very clearly how the jitter in the rotation angles θ_x and θ_y is affected by the actual pose of the coplanar marker cluster. Especially a (near) top view at the cluster, which is a very common configuration in a real setup, reveals an intense source for jitter in these rotation angles. This further translates to a jitter of more than one millimeter of the chosen target point, caused by the leverage effect of the error in the rigid body transformation. Choosing a non-coplanar marker cluster can greatly improve the accuracy of θ_x and θ_y. The jitter of the target point reduces to about 0.3 mm.

These results basically confirm that, in terms of accuracy, the worst case for a coplanar marker cluster occurs when it is viewed from the top. In general a non-coplanar cluster delivers a much more consistent error distribution that is comparable with the best case scenario of a coplanar cluster.

3.6. Experimental Variation of the Cluster Pose

To verify the results of the computer modeled marker clusters we build two marker clusters, one coplanar and one non-coplanar. Their design is similar to the ones used in the simulations in the previous section. We use these two marker sets for tracking and record the estimated pose of our real-time tracker for 1000 samples while the marker cluster is stationary fixed. We repeat this test for different poses by varying the angle between the x-y plane of the marker cluster and the x-y plane of the tracking camera from 0˚to 45˚. The resultant jitter of the pose and consequently the projection of the 95% confidence ellipsoid of the target point (as chosen in the previous sections) are depicted in Figure 6 and Figure 7 for the coplanar and the non-coplanar marker cluster, respectively.

The similarity of these error graphs with the ones of the simulation in Section 3.5 validates the choice of the noise model and confirms the correctness of the study done for the marker configuration design.

4. Summary

We characterized the tracking error of a group of markers within a single camera tracking framework. Thereby, we considered a family of circular shaped marker clusters with various parameters, i.e., number of markers, height, and radius. For comparison, we simulated the jitter of the 6D pose and the 3D location of a single target point for each cluster configuration. In this simulation, we added noise, which was already identified from the tracking system, to the 2D locations of the projected markers. The results of the Monte Carlo simulations demonstrate that both measures of error (i.e., 6D pose and 3D location jitter) decline, as the size of the marker cluster, the number of markers, and the variation in marker heights increase. More importantly, the measures of error show different sensitivities to each of the parameters of the cluster design. For example, one gains more in terms of accuracy by increasing the cluster radius rather than increasing the number of markers.

We finally selected two sets of design parameters and built one coplanar and one non-coplanar marker cluster. Then we recorded the pose of these clusters using our real-time tracking camera system and analyzed the error measures. The level of the observed jitter is very similar to the results of the simulations.

The benefit of this study is to be able to predict the resultant noise of a particular marker cluster, and know beforehand the parameters of the design that could be changed to meet given constraints. An application for a tracked non-coplanar marker cluster can be seen in Figure 8. For a medical scenario, we attached this marker cluster to a needle and used our AR setup to perform a guided needle biopsy. Placing the tracking camera and the video cameras for the scene view in an AR setup close together, as discussed in the beginning of this article, takes advantage of the fact that the 3D jitter of the marker cluster is mainly elongated along the line-of-sight. Therefore, the 3D jitter of a point projects only into a small 2D jitter in the camera plane, where the actual AR graphics are overlaid. Practical tests show the stability of the augmentation with an invisible jitter.

References

[1] A.R.T. GmbH. A. R. T. Infrared Tracking System, www.ar-tracking.de.

[2] D. K. Bhatnagar. Position trackers for head mounted display systems: A survey. Technical Report TR93-010, Department of Computer Science, University of North Carolina at Chapel Hill, 1993.

[3] R. Haralick and L. Shapiro. *Computer and Robot Vision*. Adison-Wesley, Reading, MA, 1993.

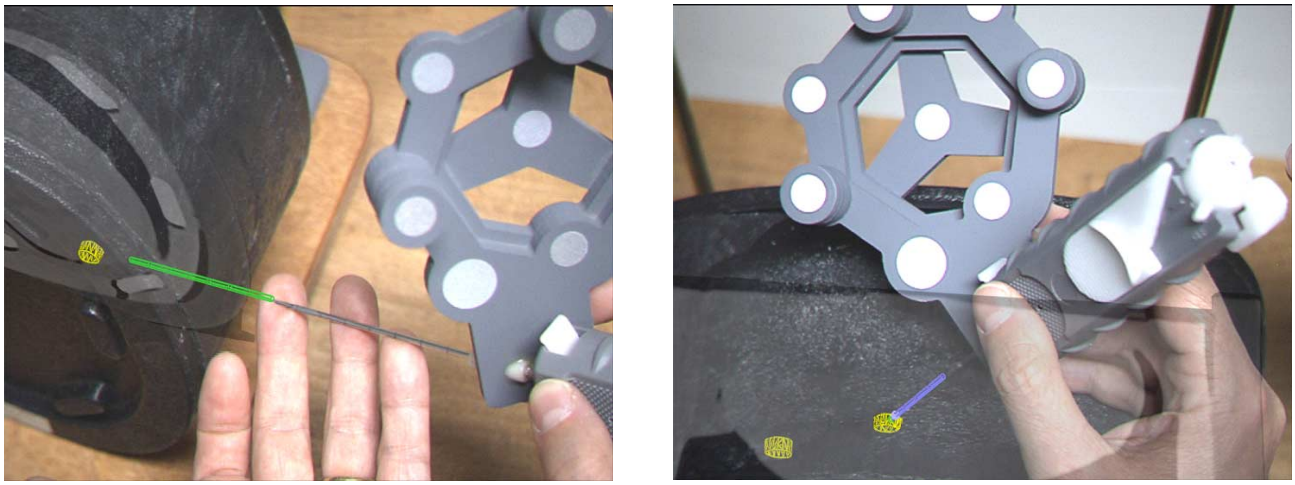

Figure 8. Medical AR scenario where an abdominal phantom (aligned in the frame marker coordinate system) and a needle (tracked with an attached marker cluster) are overlaid with graphics (CT-slice, pre-segmented lesions and visualized needle) to guide the biopsy. *(left)* **The trajectory of the needle is represented by graphics, which seems to be rigidly anchored at the needle tip.** *(right)* **The needle is inserted into the phantom, whereby the graphics of the needle are visible "through" the surface of the phantom.**

[4] R. M. Haralick, H. Joo, C. Lee, X. Zhuang, V. Vaidya, and M. Kim. Pose estimation from corresponding point data. *IEEE Transactions on Systems, Man and Cybernetics*, 19(6):1426–1446, 1989.

[5] R. Hartley and A. Zisserman. *Multiple view geometry in computer vision*. Cambridge Univ. Press, Cambridge, 2000.

[6] W. A. Hoff. Fusion of data from head-mounted and fixed sensors. In *Proc. IEEE Int. Workshop on Augmented Reality*, pages 167–182, 1998.

[7] H. Kato and M. Billinghurst. Marker tracking and HMD calibration for a video-based augmented reality conferencing system. In *Proc. IEEE Int. Workshop on Augmented Reality*, pages 125–133, 1999.

[8] R. Kumar and A. R. Hanson. Robust methods for estimating pose and a sensitivity analysis. *Comp. Vis. Graph. Im. Proc.*, 60(3):313–342, 1994.

[9] J. Rekimoto. Matrix: A realtime object identification and registration method for augmented reality. In *Asia Pacific Computer Human Interaction*, 1998.

[10] F. Sauer, A. Khamene, B. Bascle, and G. J. Rubino. A head-mounted display system for augmented reality image guidance: Towards clinical evaluation for iMRI-guided neurosurgery. In *Proc. of Medical Image Computing and Computer-Assisted Intervention*, pages 707–716, 2001.

[11] F. Sauer, A. Khamene, B. Bascle, L. Schimmang, F. Wenzel, and S. Vogt. Augmented reality visualization of ultrasound images: System description, calibration, and features. In *Int. Symp. on Augmented Reality*, pages 30–39, 2001.

[12] F. Sauer, A. Khamene, B. Bascle, and S. Vogt. An augmented reality system for ultrasound guided needle biopsies. In *Medicine Meets Virtual Reality.*, pages 455–460, 2002.

[13] F. Sauer, A. Khamene, B. Bascle, S. Vogt, and G. J. Rubino. Augmented reality visualization in iMRI operating room: System description and pre-clinical testing. In *Proc. of SPIE Conf. of Medical Imaging*, pages 446–454, 2002.

[14] F. Sauer, F. Wenzel, S. Vogt, Y. Tao, Y. Genc, and A. Bani-Hashemi. Augmented workspace: Designing an AR testbed. In *Int. Symp. on Augmented Reality*, pages 47–53, 2000.

[15] R. Y. Tsai. A versatile camera calibration technique for high-accuracy 3D machine vision metrology using off-the-shelf TV cameras and lenses. *IEEE Journal of Robotics and Automation*, 3(4):323–344, August 1987.

[16] J. Wang, V. Chi, and H. Fuchs. A real-time optical 3D tracker for head mounted display systems. In *Computer Graphics, Special issue on 1990 Symposium on Interactive 3D Graphics*, volume 24, pages 205–215. ACM SIGGRAPH, New York, March 1990.

[17] X. Zhang and N. Navab. Tracking and pose estimation for computer assisted localization in industrial environments. In *IEEE Workshop on Applications of Computer Vision*, pages 214–221, 2000.